In-situ high-resolution measurement of RHF nuclear fuel plates' spacing

Ghita Zaz, Emmanuel Le Clézio, Ali Dekious, Meriem Chrifi Alaoui, Yoann Calzavara, Gilles Despaux

In-situ high-resolution measurement of RHF nuclear fuel plates' spacing

Dr. Ghita Zaz, Pr. Emmanuel Le Clézio *Member, IEEE*, Dr. Ali Dekious, Meriem Chrifi Alaoui, Dr. Yoann Calzavara and Pr. Gilles Despaux *Member, IEEE*

***Abstract*—Most of the High Performance Research Reactors (HPRR) are made of plates undergoing a limited swelling during irradiation. Measuring the fuel thickness or the inter-plate distance is then a promissing way to obtain information on the fuel element irradiation history. The experimental constraints are however quite heavy due to the aimed resolution and the element geometry. In order to perform such measurements, a high resolution ultrasonic device was designed. It was thinned down to 1 mm in order to be inserted into the reactor water-channel. The system is then excited with a 120 MHz central frequency burst and the distance measurement is carried out through the ultrasonic waves' time of flight estimation. A series of experiments was performed on a full size irradiated fuel element of the "Institut Laue-Langevin" reactor proving the feasibility of real-time in-situ measurements.**

***Index Terms*—High frequency, high resolution, harsh environment, ultrasonic transducer, HPRR, RHF.**

I. Introduction

MOST of the High Performance Research Reactors (HPRR) use plate-type fuels where the fissile material is dispersed in a matrix within an alloy cladding [1]. During irradiation, a limited swelling of the plates may appear, bearing information on the element irradiation history. In the framework of a conversion study of its High Flux Reactors (RHF) into Low Enriched Uranium, the Institut Laue-Langevin (ILL) [2] launched a study aiming to the development of tools allowing the assessment of the fuel plate structural modifications. In particular, to perform precise water-channel thickness measurements, the current Post Irradiation Examination methods require disassembling the fuel element, i.e. cutting the fuel plates. The present paper aims at developing a non-destructive in-situ control device.

Due to the microscopic nature of the fuel plate transformations, a micron-scale study is needed while the fuel arrangement limits the inter-plate distance to less than two millimeters. Moreover, the fuel element is generally situated well below the surface of a moderating pool yielding a very difficult access. Finally, the measurement devices undergo high-levels of radiations.

Several methods can be considered to perform distance measurements. Optical [3]-[5], magnetic [6]-[10], capacitive [11], or electromagnetic [12] devices might be relevant and reach today the nanometer resolution even in high-temperature and/or high-pressure environments. However, while some of them possess a low sensitivity to some environmental conditions such as pressure and temperature, most of these systems present drawbacks conflicting with in-situ measurements inside RHF fuel elements. In particular, they may be too cumbersome to be integrated into the water-channel, may not be submerged or are deeply affected by highly radiative environments.

To take into account the experimental constraints, the development and test of a double-sided high-resolution ultrasonic device is here proposed. It includes transducers integrated on both sides of a blade with the constraint of a 1 mm total device thickness and designed with nuclear specifications. To achieve the expected resolution, the system is associated to a set of high frequency acquisition instruments and excited by bursts with a 120 MHz central frequency. At these high frequencies, the ultrasonic wavelength is sensitive to the layered structure of the devices and their design plays a central role in the shape of transmitted and received signals. To understand their behavior, the sensors are then modeled through the transfer matrix method [13]-[17]. Through a pulse-echo protocol, the device then allows distance measurements through the recording of the time of flight t (ToF) of the signals reflected by the fuel plates surfaces [18], [19]. To infer distance estimations from this measurement, a spectral analysis of the sensor response is proposed to identify the ultrasonic velocity in the water of the cooling channel at the measurement points.

Proving the feasibility of the in-situ distance measurements, experiments were performed on a RHF spent fuel element, demonstrating that the different components of the ultrasonic transducers showed good resistance to radiations allowing a signal to noise ratio sufficient to obtain a first in-situ estimation of the inter-plate distance.

The first section of the paper presents the sensor and device conception as well as the signal processing allowing the estimation of the ultrasonic ToF. The modeling of the sensor behavior is then proposed in

Ghita Zaz is with INSA of the Euromed University of Fes, BP 51, Fes, Maroco.

Emmanuel Le Clézio*, Meriem Chrifi Alaoui and Gilles Despaux are with University of Montpellier, IES UMR 5214, 860 Rue Saint Priest, CC 05 003, F-34000 Montpellier.

Emmanuel Le Clézio*, Meriem Chrifi Alaoui, Ali Dekious and Gilles Despaux are with CNRS, IES UMR 5214, 860 Rue Saint Priest, CC 05 003, F-34000 Montpellier.

Yoann Calzavara is with the Institut Laue Langevin - ILL, 71 Avenue des Martyrs, 38000 Grenoble, France (e-mail: calzavara@ill.fr).

Corresponding author Emmanuel Le Clézio: +0-033-467-143-702; fax: +0-033-467-149-252; e-mail: emmanuel.le-clezio@umontpellier.fr

the second section while the temperature dependance of the ultrasonic velocity of the waves propagating in the cooling pool water is studied in the third. The last section of the paper deals with the results and discussion on the experiments performed on one full size irradiated fuel element of a RHF.

II. Sensor and device conception

A. Experimental constraints and proposed sensor conception

The experimental constraints associated with an in-situ control of the fuel element are quite heavy. Regarding the RHF element presented in section VI-A, the inter-plate distance corresponding to the width of the cooling water-channel is of 1800 μm clearly limiting the possible thickness of the measuring device. Moreover, measurements have to be performed 5 m underwater in a highly radiative environment and are expected to possess a resolution of the order of the micron.

To overcome the above difficulties, the development of a high frequency ultrasonic device is here proposed. Generally speaking, ultrasonic techniques yield high levels of performance and are radiation resistant [20]. Sensors can be sealed to be immersed and can be designed to reach the expected dimensions.

Distance measurements are usually based on time of flight estimations where the time delay separating two ultrasonic signals is directly linked to the distance via the velocity of the ultrasonic wave inside the medium. Several means allow this identification. The Phase Shift Method (PSM) implies the identification of the phase difference between transmitted and received continuous waves [15], [21], [22]. This method can be very accurate and overcomes issues of traditional acoustic attenuation. However, phase ambiguity will occur if the propagation path exceeds a full wavelength clearly limiting the resolution or the applicability of the expected device.

An alternative is here proposed through the implementation of a pulse-echo method [18], [19]. Due to the experimental constraints, a device working in a reflection mode is proposed. It includes a pair of waterproof transducers integrated into the thickness of both sides of a stainless steel blade thin enough to be inserted into the width of the water-channel (Figure 1.(a)). Each transceiver emits an ultrasonic signal in water and receives its echoes reflected from the facing plate. Knowing the speed of sound c in water and the thickness h of the blade, the total distance d between the plates can be obtained by the determination of the ToF t_1 and t_2 of the two ultrasonic signals generated and received by each transducer:

$$d = h + c\left(\frac{t_1 + t_2}{2}\right). \quad (1)$$

B. Experimental set-up

1) Device geometry: To respect the experimental constraints, the ultrasonic transducers are mounted on one end of a 1 mm thick, 10 mm wide and 1500 mm long stainless steel nuclear qualified blade as presented in Figure 1.(b). This latter is connected to a 5 m long stainless steel tube with a 22 mm diameter acting as a handling device. A close view of the end of the blade including the transducers is presented in Figure 1.(c). The transducer locations are 500 μm deep circular grooves including a central hole allowing the manufacturing of the sensors connections and backings. The flat borders act like a resting zone for a $LiNbO_3$ piezoelectric disc corresponding to the active element of the sensor. To set up the cables, a groove is drilled on both faces of the blade. The connections are made possible thanks to notches positioned on the blade side.

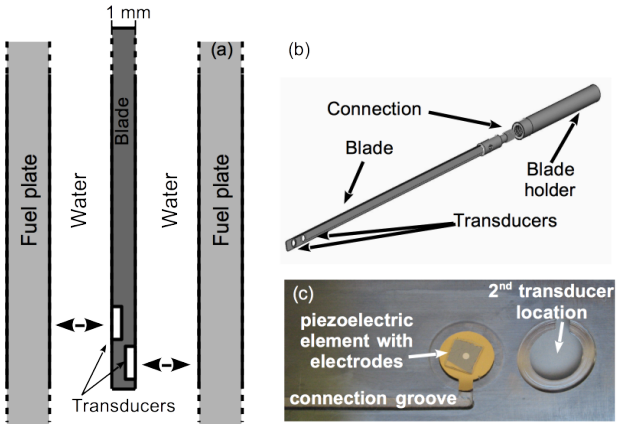

Fig. 1. (a) General principle of inter-plate distance measurement and geometry of the sensor holder: (b) device holder and blade; (c) image of the end of the blade with one inserted transducer.

2) Transduction elements: Both transducers possess the multilayered structure presented in Figure 2. They are composed of a $LiNbO_3$ piezoelectric element thinned down to 30 μm in a way to operate with a frequency bandwidth extending beyond 120 MHz. This disc is welded on one surface to a gold and chrome electrode and is glued to a 400 μm thick silica delay line. An aluminum layer is deposited on the second surface as an electric input and output electrode. Finally, the back surface of the transducer is covered by a filled epoxy resin layer acting like a backing material absorbing the vibration of the rear face of the piezoelectric element and ensuring forward propagation.

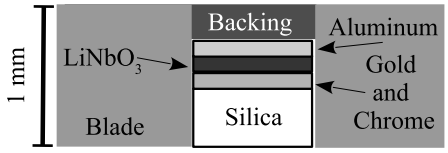

Fig. 2. Ultrasonic transducer structure.

3) Acquisition system: To allow the emission and reception of ultrasonic signals at very high frequencies, the electronic acquisition chain includes among others:

- A dual transmitter/receiver electronic system

specifically designed to improve the excitation signal of the transducers,
- Two RF NI PXIe-5690 preamplifier cards with a $[10^2 - 3 \cdot 10^9]$ Hz bandwidth,
- A NI PXIe-5162 acquisition card sampling at 5 GS/s with a resolution of 10 bits and a 1.5 GHz bandwidth.

At the high working frequencies of the device, the structure of the multilayered sensor is of the order of the ultrasonic wavelength and plays a crucial role in the shape of transmitted and received signals. Their complex nature (presented in section IV-A of the present paper) and the expected resolution then imply a close understanding of the structure of the sensor ultrasonic signature. The modeling of the acoustic behavior of the transducers is then proposed in the following section.

III. Modeling of the Sensor Ultrasonic Behavior

A. Ultrasound propagation in multilayered structures

The modeling of the ultrasonic wave propagation is based on the Stroh formalism [23]-[26] associated with a recursive implementation of the hybrid matrix [27]. While a detailed presentation of the method is presented in a previous work [17], a quick overview is proposed hereafter. N layers, piezoelectric or not, are stacked in the $\mathbf{z}$ direction as in Figure 3. Each homogeneous layer

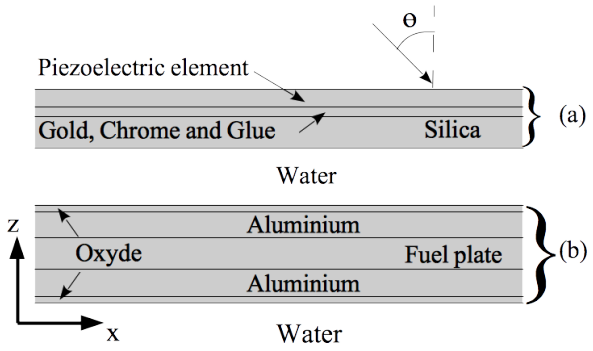

Fig. 3. The modeled multilayer medium: (a) sensor and (b) fuel element structures.

m is of thickness h_m, of density ρ_m and of elastic $\mathbf{C}_m$, piezoelectric $\mathbf{e}_m$ and dielectric $\boldsymbol{\varepsilon}_m$ tensors referred to some crystallographic basis. In one layer, the system of governing equations of acoustic wave propagation is:

$$\begin{aligned} &\sigma_{ij,j} = \rho \ddot{u}_i, \quad d_{i,i} = 0, \\ &\sigma_{ij} = C_{ijkl} u_{k,l} + e_{kij} \varphi_{,k}, \\ &d_i = -\varepsilon_{ij} \varphi_{,j} + e_{ijk} u_{j,k} \end{aligned} \tag{2}$$

where the index m is omitted for convenience. $\boldsymbol{\sigma}$ is the mechanical stress tensor, $\mathbf{u}$ is the elastic displacement, and d and φ are the induction and potential of the electric field induced by the piezoelectric effect. Steady time-harmonic motion inducing a $e^{i\omega t}$ time dependence is assumed along an arbitrary direction parallel to the surfaces of the plate and taken as the $\mathbf{x}$-axis. $(\mathbf{m}, \mathbf{n}) = (\mathbf{x}, \mathbf{z})$ is the sagittal plane and solutions to (2) are sought in the form:

$$\begin{aligned} &\mathbf{u} = \mathbf{A}(z) e^{ik(x-vt)}, \quad \boldsymbol{\sigma}\mathbf{n} = \mathbf{F}(z) e^{ik(x-vt)}, \\ &\varphi = \phi(z) e^{ik(x-vt)}, \quad d = D(z) e^{ik(x-vt)}, \end{aligned} \tag{3}$$

where $k(>0)$ is the wavenumber along the $\mathbf{x}$-axis, v is the phase velocity, and $\omega = kv$ is the angular frequency. The octet formalism of piezoelectric [24]-[26] incorporates (2), (3) into the first-order ordinary differential system (ODS):

$$\left[\mathbf{Q}(z) - \frac{d}{dz} \right] \boldsymbol{\eta}(z) = \mathbf{0}, \tag{4}$$

where $\mathbf{Q}$ is the system matrix. The eight-component state vector $\boldsymbol{\eta}$ is expressed as follows:

$$\boldsymbol{\eta} = \begin{pmatrix} \mathbf{U} \\ \mathbf{V} \end{pmatrix}, \quad \mathbf{U} = \begin{pmatrix} \mathbf{A} \\ \phi \end{pmatrix}, \quad \mathbf{V} = ik^{-1} \begin{pmatrix} \mathbf{F} \\ D \end{pmatrix}. \tag{5}$$

In each layer m, the eight up-going and down-going bulk waves are solutions of equation (4) and can be expressed through the eigen-spectrum of the system matrix $\mathbf{Q}_m$ [28], [27], [17]. For each layer m, the field vector elements can then be linked through the following matrix relation:

$$\begin{bmatrix} \mathbf{U}_m(z_{m-1}) \\ \mathbf{V}_m(z_m) \end{bmatrix} = \mathbf{H}^m \begin{bmatrix} \mathbf{V}_m(z_{m-1}) \\ \mathbf{U}_m(z_m) \end{bmatrix}, \tag{6}$$

where z_{m-1} and z_m are respectively the lower and upper surface of the m^{th} layer. $\mathbf{H}^m$ is called the layer hybrid compliance-stiffness matrix, or simply layer hybrid matrix. Its expression in terms of its eigen-solutions can be found in [17]. It can be decomposed into 4 blocks of 4×4 matrices:

$$\mathbf{H}^m = \begin{bmatrix} \mathbf{H}^m_{11} & \mathbf{H}^m_{12} \\ \mathbf{H}^m_{21} & \mathbf{H}^m_{22} \end{bmatrix}. \tag{7}$$

The hybrid matrix $\mathbf{H}^m$, $m = 1 \ldots N$, of each layer being known the global hybrid matrix is recursively constructed from the top layer $(m = N)$ to the bottom one $(m = 1)$ [27], [17]:

$$\mathbf{H}^{(m)}_{11} = \mathbf{H}^m_{11} + \mathbf{H}^m_{12} \mathbf{H}^{(m+1)}_{11} \mathbf{J}^{-1}_m \mathbf{H}^m_{21}, \tag{8}$$

$$\mathbf{H}^{(m)}_{12} = \mathbf{H}^m_{12} \{ \mathbf{I} + \mathbf{H}^{(m+1)}_{11} \mathbf{J}^{-1}_m \mathbf{H}^m_{22} \} \mathbf{H}^{(m+1)}_{12}, \tag{9}$$

$$\mathbf{H}^{(m)}_{21} = \mathbf{H}^{(m+1)}_{21} \mathbf{J}^{-1}_m \mathbf{H}^m_{21}, \tag{10}$$

$$\mathbf{H}^{(m)}_{22} = \mathbf{H}^{(m+1)}_{22} + \mathbf{H}^{(m+1)}_{21} \mathbf{J}^{-1}_m \mathbf{H}^m_{22} \mathbf{H}^{(m+1)}_{12}, \tag{11}$$

with $\mathbf{J}_m = [\mathbf{I} - \mathbf{H}^m_{22} \mathbf{H}^{(m+1)}_{11}]$. The superscript (m) in brackets denotes the stack matrix for layers from m to N. The global hybrid matrix is given by the recursive algorithm starting from layer N down to layer 1. The transmission coefficients of acoustic plane waves propagating through multilayered media immersed in a non-viscous fluid are then expressed through the global admittance matrix $\mathbf{Y}$ of the structure as presented in [17] :

$$\mathbf{Y} = i \begin{bmatrix} \mathbf{H}^{(1)}_{12} (\mathbf{H}^{(1)}_{22})^{-1} \mathbf{H}^{(1)}_{21} - \mathbf{H}^{(1)}_{11} & \mathbf{H}^{(1)}_{21} (\mathbf{H}^{(1)}_{22})^{-1} \\ (\mathbf{H}^{(1)}_{22})^{-1} \mathbf{H}^{(1)}_{21} & (\mathbf{H}^{(1)}_{22})^{-1} \end{bmatrix}. \tag{12}$$

To take into account physical and dimensional parameters of each plate, the model requires as numerical input data the elastic, piezoelectric and dielectric constants of the media, their volume densities and the layer thicknesses. As presented in the next section, the above model has been implemented to understand the behavior of the ultrasonic signals propagating in the multilayered medium noted (a) in Figure 3. It includes the transducer layers (the piezoelectric element, the golden and aluminium electrodes, and the delay line of silica), the water-channel, and the fuel plate.

B. Modeling of the sensor ultrasonic response

The complex transmission coefficient $T(\omega_n)$ of each plane wave propagating through the sensor structure is computed as presented above for each frequency $\omega_n = 2\pi f_n$, $n = 1 \dots N$ inside the sensor bandwidth. A Fourier summation is then implemented to reconstruct the temporal signal backscattered to the sensor taking into account the initial amplitudes $A(\omega_n)$ of each frequency in the transducer spectrum:

$$s(t) = \sum_{n=1}^{N} A(\omega_n) T(\omega_n) e^{i\omega_n t}. \quad (13)$$

C. Comparison between experimental and simulated signals

1) Transducer response: The temporal signal $s(t)$ of equation (13) is presented as dashed lines in Figure 4. The different bursts that can be observed correspond to multi-reflections on the silica/water interface of the initial signal generated by the piezoelectric element, the progressive transmission of ultrasonic energy into the water yielding the decreasing of the amplitudes of the echoes.

This theoretical signal is compared to the experimental one, presented in straight lines. To obtain the very good agreement between these two signals, a fitting procedure has been implemented allowing the identification of the thickness of each layer constituting the sensor. This allowed both the characterization of the device behavior and the understanding of the influence of each layer on the global signal structure in view of a sensor optimization. Differences can be noticed between the two signals, in particular in the amplitude of the two first pulses, the experimental ones being much smaller than the simulated ones. This is due to instrumentation constraints imposing a high attenuation of the first echoes to avoid a saturation of the high voltage electronics.

IV. Time of Flight estimation

A. Propagation through the total structure

To envision water-channel thickness measurements, the above simulations are extended to consider as in Figure 3 the propagation of the ultrasonic waves into the water, their reflections onto the surface of the fuel element and their back-propagations to the sensor. Results are presented in Figure 5.

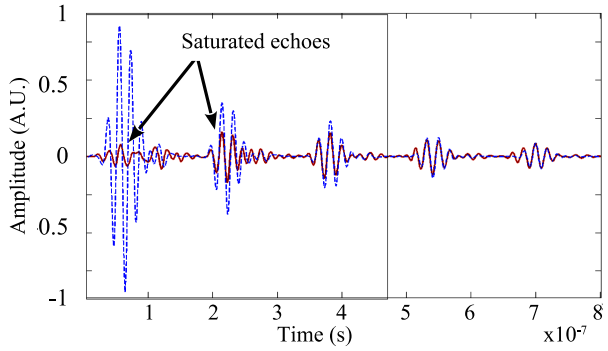

Fig. 4. Reflection of the signals within the multilayer structure of the transducer. Dashed line: Theoretical. Solid line: measured

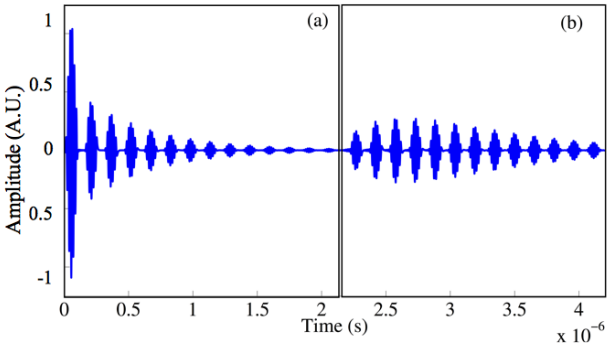

Fig. 5. Simulated signals corresponding to the propagation of the ultrasonic waves into the water and their back-propagations to the sensor, showing two series of echoes: (a) reflection of the signals within the multilayer structure of the transducer; (b) dual series obtained after propagation in the water-channel and reflection on the fuel plate.

The first part, noted (a), corresponds to the sensor signature of Figure 4. This composite signal is transmitted into the water and reflected back to the sensor by the surface of the nuclear fuel plate. The corresponding signal is presented in part (b) of Figure 5. Some differences in the structure of these two sets of burst can be observed, in particular the amplitude of the two first ones of part (b) is lower than the following ones. The simulation proved that this behavior is due to the presence of the glue layer, the first echo amplitude being linked to its thickness. To estimate the water-channel thickness, the determination of the ToF between parts (a) and (b) of Figure 5 is proposed in the next section.

B. Signal processing

One of the simplest forms of ToF estimation is the threshold method. This technique proposes to identify the arrival of an acoustic signal to the time where its amplitude exceeds a given amplitude level. Thresholding systems do not require any complex computations, but their precision can be degraded for low signal-to-noise ratio (SNR) [19], [29]-[32]. It is here proposed to perform the ToF estimation through a cross-correlation

method [31]-[36] computed between the two parts (a) and (b) of the signal of Figure 5, respectively denoted $x(t)$ and $y(t)$. Their cross correlation $R_{xy}(t)$ is defined by the following equation:

$$R_{xy}(t) = x(t) \otimes y(t) = \int_{-\infty}^{\infty} x(\tau)y(t+\tau)d\tau. \quad (14)$$

Taking into account the structure of the ultrasonic signals of Figure 5, equation (14) becomes

$$R_{xy}(t) = \sum_{i=1}^{n} x_i(t) \otimes \sum_{j=1}^{n} y_j(t) \quad (15)$$

where $x_i(t) = a_i s(t-i\tau)$ and $y_j(t) = b_j s(t-j\tau-\theta)$, τ and θ corresponding to the delays due to the ultrasonic wave propagation in silica and water, respectively. a_i and b_j are the echoes' amplitudes of the elementary bursts $s(t)$. Finally,

$$R_{xy}(t) = \sum_{i=1}^{n}\sum_{j=1}^{n} a_i b_j s(t-i\tau) \otimes s(t-j\tau-\theta). \quad (16)$$

Compared to the correlation $abs(t) \otimes s(t-\theta)$ of two single bursts of amplitudes a and b separated by the ultrasonic time of flight in water θ, the estimation of the maximum of similarity of the two composite signals is here optimized through the contribution of each pair of bursts increasing the signal to noise ratio.

V. The temperature dependance of the ultrasonic velocity $c(T)$

The above relation (16) allows a precise identification of the time delay corresponding to ultrasonic propagation to and from the fuel plates back to the sensor. To correctly infer distance estimations from this measurement, a precise knowledge of the ultrasonic velocity in the water of the cooling channel must be obtained. To do so, we propose in this section to take advantage of the thermal influence of the environment onto the sensors.

A. Temperature measurement

The spectral components of the sensors being directly dependent on the thermal expansion of transducers layers, a frequency analysis of the device response is now proposed in a way to infer the temperature at the measurement point.

1) Device structure modifications: When immersed into water, the sensor temperature variations lead to a thermal expansion or shrinkage of its multi-layered structure, yielding in particular modifications in its piezoelectric element and silica delay line thicknesses. On the expected temperature range of a cooling pool (from 25 ˚C to 35 ˚C), the thermal expansion coefficient α_{Si} of the silica is $4.1{\cdot}10^{-5}$/˚C [37], [38] and that of the piezoelectric element ranges between $\alpha_{LiNb0_3} = 7.5 \cdot 10^{-4}$/˚C and $\alpha_{LiNb0_3} = 15 \cdot 10^{-4}$/˚C [39]. These values show that it is possible to neglect the thermal expansion of the silica, the piezoelectric element being mainly responsible of a change of the transducer resonant frequency. The thermal modifications of the other layers of the sensor are here omitted due to their very small thicknesses yielding negligible modifications in the device response.

The thermal expansion of the piezoelectric element causes a change of its resonant frequency. Indeed, when the piezoelectric element is heated, its thickness d changes according to the thermal expansion law, which can be written as [40]:

$$d(T_i) = d(T_{i-1}) + \delta d \quad (17)$$

where

$$\delta d = \alpha \delta T d(T_0). \quad (18)$$

The thickness of the piezoelectric element is directly related to its resonant frequency by the following equation:

$$f = \frac{v}{2d} \quad (19)$$

where v is the ultrasonic velocity of the longitudinal wave propagating inside the piezoelectric element. As a consequence,

$$\delta f = 0.5\frac{\delta v \cdot d - v\delta d}{v^2}. \quad (20)$$

On the proposed temperature range, $\delta v \approx 0$. We can then deduce that:

$$\delta f = -0.5\frac{\delta d}{v} \quad (21)$$

leading to transducer frequency changes according to the following equation:

$$f(T_i) = f(T_{i-1}) + \delta f. \quad (22)$$

A simulation based on the above equation was developed to anticipate the behavior of the frequency transducer according to the temperature and to evaluate the accuracy of the measurement system. Results are presented as dots in Figure 6.

2) Device calibration: A measurement system has then been implemented to confirm the above result. The ultrasonic device of Figure 1 is inserted into a thermostatic bath filled with deionized water similar to that of the cooling pool of the RHF reactor. The temperature is then cooled down from 35 ˚C to 10 ˚C by steps of 0.5 ˚C. Each step is maintained several minutes to ensure temperature stability within the sensor. The transducer is then excited by the system presented in section II-B3 and its frequency response is acquired. Acquisitions of the water temperature are also performed thanks to a thermocouple. Results are compared with good agreement in Figure 6 to the simulations confirming that the frequency variation of the sensor is mainly controlled by the piezoelectric element thermal expansion.

From 10 ˚C to 35 ˚C, the resonance frequency of the transducer is decreased by 4.3 MHz. While controlling the RHF structure, this experimental calibration law will be used to determine the in-situ temperature of the water-channel from the resonant frequency of the sensor.

B. Ultrasonic velocity measurement

The temperature being evaluated at the measurement point, the next step deals with the identification of the thermal dependance of velocity of the ultrasonic wave propagating in the water pool. To do so, a home-made quartz tank with a controlled thicknesses of 1800 ± 10 μm is used as reference reflector and the ToF is measured by the above device in the $[10 - 35]$ °C range by steps of 0.1 °C. The ultrasonic velocity variation with the temperature is presented in Figure 6 and compared to values proposed in [41].

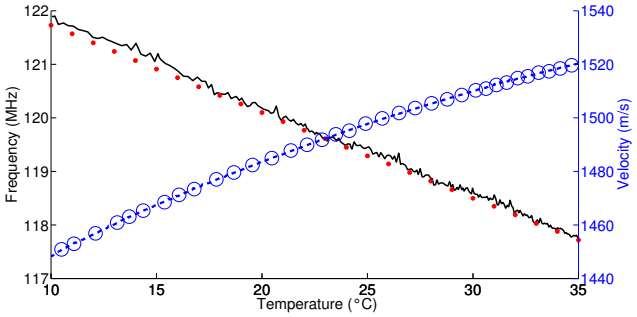

Fig. 6. Variations with the temperature of the sensor response frequency (straight line: experimental data; dots: modeling) and of the ultrasonic velocity (dashed line from [41]; circles: experimental data).

C. Distance estimation

The two experimental laws of Figure 6 allow a real-time in-situ estimation of the local ultrasonic wave velocity at the measurement point through the measurement of the resonant frequency of the sensor. Then, with known local time of flight and ultrasonic velocity, the water-channel width d can be calculated from equation (1). The uncertainty δd on its estimation is given by:

$$\delta d \quad = \quad d \times \left(\frac{\delta t}{t} + \frac{\delta v}{v} \right) \tag{23}$$

where δt and δv are respectively the absolute uncertainty of the time of flight and of the ultrasonic velocity measurements. The maximum difference between experimental and theoretical velocities presented in Figure 6 being of about 4 m/s, the total error on the inter-plate distance estimation is estimated in our experiments to less than 20 μm.

VI. In-situ measurements

A. The fuel element structure

The High Flux Reactor of the Laue-Langevin Institute is a research reactor that produces neutrons for fundamental science experiments. Heavy water is used as a moderator in order to slow down the neutrons produced by the fission reaction allowing the generation of the most intense continuous flux of thermal neutrons, about $1.5 \cdot 10^{15}$ neutrons per second per cm^2, with a thermal power of 58 MW. The RHF fuel element is made of 280 aluminum curved plates containing high-enriched uranium aluminide-aluminum (UAlx/Al) dispersion fuel and forming a cylindrical tube (Figure 7.(a)). The plates possess the following dimensions: 903 mm long, 69.54 mm wide and a nominal thickness of 1.27 mm. They are regularly spaced by a 1.8 mm wide channel where a water stream flows as coolant and moderator to the nuclear reaction (see Figure 7.(b)).

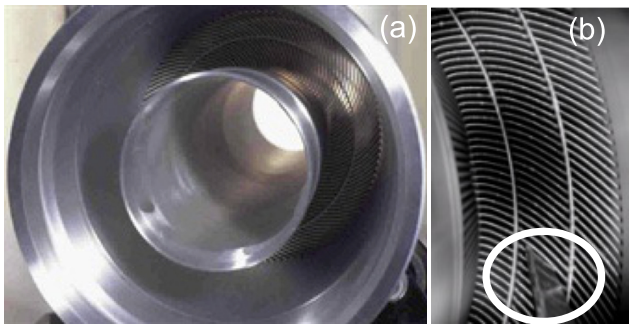

Fig. 7. (a) Top view of a mockup of the ILL RHF fuel element; (b) Fuel element plates' arrangement and ultrasonic sensor position.

B. Environment

To validate the distance measurement approach, an in-situ experiment was carried out in the above RHF positionned 5 m under water in a cooling pool. To evaluate the radiation resistance of the device and estimate the measurement resolution achievable in a highly radiative environment, measurements have been performed inside three different water-channels in which the sensor was first moved down to a depth of about 10 cm. During the experiment, the mean water-channel temperature was measured equal to 28.3 ± 0.1 °C.

C. Results

In each channel, acoustic signals were recorded every 50 ms while slowly manually ascending the device. As previously mentioned, the experimental constraints associated with an in-situ control are quite heavy. In particular, the device has to be handled by an operator situated over the cooling pool. One of the consequences linked to this experimental implementation deals with the control of the ultrasonic fields' alignment with the normal of the reflecting surfaces. To illustrate this point, Figure 8 presents the energy of the reflected signals received in one of the water-channel by one of the sensors. It clearly shows that, when the sensor is not correctly oriented, the amplitude of the acquired signal is greatly degraded. The influence of this misalignment on the thickness estimation has been quantified through the model presented in section III-A and [13]-[17] and it was found that due to the fuel plates' curvature, the maximum inclination of the transducer is less than $3°$ yielding a maximum error of 4 μm on the global distance estimation. However, while the sensors alignment is

clearly an issue due to the experimental constraints, results from Figure 8 give an indication of the quality of the measurements. As a consequence, the energy of each signal is being computed and used to select relevant signals yielding reliable identifications of the water-channel thickness. The corresponding estimations

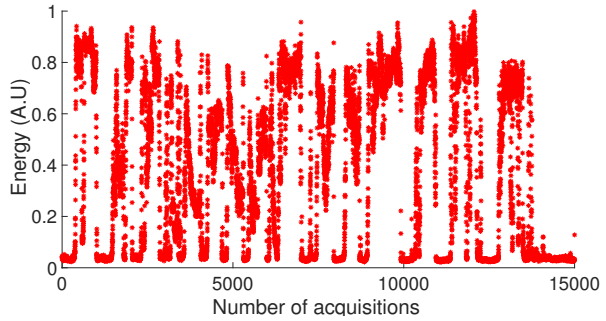

Fig. 8. Evolution during the acquisition process of the energy of the reflected signals measured by one of the sensors.

are presented in 9 where spurious points corresponding to signals with low energy have been removed.

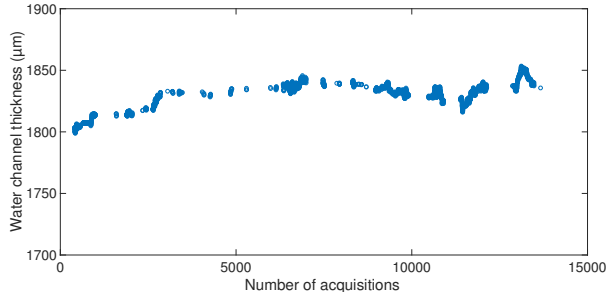

Fig. 9. Inter-plate distance measurements where spurious points corresponding to low energy signals have been removed.

D. Discussion

First of all, these results clearly prove the feasibility of a in-situ non destructive control of the RHF thanks to an ultrasonic method. Indeed, the experiments demonstrated that the different components of the ultrasonic transducers showed good resistance to radiations during at least 5 hours. Moreover, in spite of the highly irradiative nature of the environment, the quality of the ultrasonic signals was sufficient to ensure a stable identification of the inter-plate distances.

Some remarks can however be made on the quality of the above results. It is here important to emphasize that due to the manual positioning of the device and the removing of the low energy signal no information on the sensor depth can be here obtained and the reader should avoid to draw a mental line between the measurements. These results however allow the estimation of a mean water-channel thickness, here equal to 1829 ± 11 μm. Moreover, the resolution of the device can be estimated thanks to the dispersion of neighboring points corresponding to measurements performed at very close locations. It is here estimated to 2 μm.

VII. Conclusion

This paper presented a prototype of a ultrasonic device integrating two high frequency transducers designed to measure water-channel thickness variations inside a High Flux Reactor positioned 5 meters below the water surface of a cooling pool. With a total thickness of 1 mm, the device is attached to a holder to allow its insertion into the nominally 1800 μm thick water-channel of the fuel element. To achieve the expected resolution, the system is excited with frequencies up to 120 MHz and integrated into a set of high frequency acquisition instruments. Knowing the speed of sound in water, the device allows the distance measurement through the evaluation of the ultrasonic wave's time of flight. To do so, the influence of the thermal expansion of the transducer layers on its resonant frequency is taken into account to infer the local temperature, and the corresponding ultrasonic wave velocity, at the measurement point. A first experiment was performed in the High Flux Reactor of the Laue-Langevin Institute, allowing the identification of the in-situ experimental constraints. Moreover, the corresponding results clearly proved the resistance of the sensor components to the radiations and demonstrated the feasibility of the distance measurement in a highly radiative environment. Future works will deal with the improvement of the measurement reliability. In particular, to study the sensor behavior under gamma radiations and the potential evolution of its characteristics, three transducers will be tested in an irradiation chamber. An automated system supporting the transducers and a guiding system are moreover being designed to ease the insertion of the blade into the fuel element and stabilize its position between the fuel plates. Associated to a control of the position of the sensor, it should allow quantitative measurements of the water-channel variations along a vertical generating line of the fuel-element-water-channel.

Acknowledgment

The authors would like to thank Laurent Podevin, Yannick Launay and Alain Portal, respectively assistant engineer, technician and study engineer at the IES - UMR CNRS 5214, for their strong contributions to manufacture the sensors and the associated electronics.

References

[1] Leo Sannen, Sven van den Berghe, Ann Leenaers, and Edgar Koonen. From High to Low Enriched Uranium Fuel in Research Reactors. In *5th Forum on new materials part B*, volume 73 of *Advances in Science and Technology*, pages 78–90. Trans Tech Publications, 2011.

[2] Institut Laue-Langevin. https://www.ill.eu.

[3] J. Thiel, T. Pfeifer, and M. Hartmann. Interferometric measurement of absolute distances of up to 40 m. *Measurement*, 16(1):1 – 6, 1995.

[4] V. Lombardo, T. Marzulli, C. Pappalettere, and P. Sforza. A time-of-scan laser triangulation technique for distance measurements. *Optics and Lasers in Engineering*, 39(2):247 – 254, 2003. Optics in Italy {III}.

[5] Markus-Christian Amann, Thierry Bosch, Marc Lescure, Risto Myllyla, and Marc Rioux. Laser ranging: a critical review of usual techniques for distance measurement. *Optical Engineering*, 40(1):10–19, 2001.

[6] S. M. Djuric, M. S. Damnjanovic, L. F. Nagy, L. D. Zivanov, and N. M. Djuric. Displacement inductive sensor: Simulation tool algorithm. In *EUROCON 2009, EUROCON '09. IEEE*, pages 671–676, May 2009.

[7] M. Jagiella and S. Fericean. Miniaturized inductive sensors for industrial applications. In *Sensors, 2002. Proceedings of IEEE*, volume 2, pages 771–778 vol.2, 2002.

[8] G. Lemarquand. A variable reluctance sensor. *IEEE Transactions on Magnetics*, 25(5):3827–3829, September 1989.

[9] G. Y. Tian, Z. X. Zhao, R. W. Baines, and P. Corcoran. Blind sensing [eddy current sensor]. *Manufacturing Engineer*, 76(4):179–182, August 1997.

[10] W Yin and J. Peyton. Thickness measurement of non-magnetic plates using multi-frequency eddy current sensors. *NDT E Int.*, 40(1):43–48, 2007.

[11] Masahiko Sakai. Capacitive Sensors. In David Havelock, Sonoko Kuwano, and Michael VorlÃd'nder, editors, *Handbook of Signal Processing in Acoustics*, pages 1339–1345. Springer New York, New York, NY, 2008.

[12] A. S. Morris. 13 - Sensor technologies. In *Measurement and Instrumentation Principles (Third Edition)*, pages 247–270. Butterworth-Heinemann, Oxford, a. s. morris edition, 2001.

[13] William T. Thomson. Transmission of Elastic Waves through a Stratified Solid Medium. *Journal of Applied Physics*, 21(2):89–93, 1950.

[14] N. A. Haskell. The dispersion of surface waves on multilayered media. *Bulletin of the Seismological Society of America*, 43(1):17–34, 1953.

[15] D. L. Folds and C. D. Loggins. Transmission and reflection of ultrasonic waves in layered media. *The Journal of the Acoustical Society of America*, 62(5):1102–1109, 1977.

[16] J. S. Sastry and M. L. Munjal. A transfer matrix approach for evaluation of the response of a multi-layer infinite plate to a two-dimensional pressure excitation. *Journal of Sound and Vibration*, 182(1):109 – 128, 1995.

[17] M. Lam, E. Le Clézio, H. Amorin, M. Alguero, Janez Holc, Marija Kosec, A. C. Hladky-Hennion, and G. Feuillard. Acoustic wave transmission through piezoelectric structured materials. *Journal of Applied Physics*, 49:424–431, 2009.

[18] D. Marioli, E. Sardini, and A. Taroni. Ultrasonic distance measurement for linear and angular position control. *IEEE Transactions on Instrumentation and Measurement*, 37(4):578–581, December 1988.

[19] D. Marioli, C. Narduzzi, C. Offelli, D. Petri, E. Sardini, and A. Taroni. Digital time-of-flight measurement for ultrasonic sensors. *IEEE Transactions on Instrumentation and Measurement*, 41(1):93–97, February 1992.

[20] D. Laux, D. Baron, G. Despaux, A.I. Kellerbauer, and M. Kinoshita. Determination of high burn-up nuclear fuel elastic properties with acoustic microscopy. *Journal of Nuclear Materials*, 420(1):94 – 100, 2012.

[21] F. E. Gueuning, M. Varlan, C. E. Eugne, and P. Dupuis. Accurate distance measurement by an autonomous ultrasonic system combining time-of-flight and phase-shift methods. *IEEE Transactions on Instrumentation and Measurement*, 46(6):1236–1240, December 1997.

[22] Ke-Nung Huang and Yu-Pei Huang. Multiple-frequency ultrasonic distance measurement using direct digital frequency synthesizers. *Sensors and Actuators A: Physical*, 149(1):42 – 50, 2009.

[23] A. N. Stroh. Steady state problems in anisotropic elasticity. *J. Math. and Phys.*, 41:77–103, 1962.

[24] E. Edgar Kraut. New Mathematical Formulation for Piezoelectric Wave Propagation. *Phys. Rev.*, 188(3):1450–1455, December 1969.

[25] J. Lothe and D. M. Barnett. Integral formalism for surface waves in piezoelectric crystals. Existence considerations. *Journal of Applied Physics*, 47(5):1799–1807, 1976.

[26] E. L. Adler. Matrix methods applied to acoustic waves in multilayers. *IEEE Trans. Ultrason. Ferroelect. Freq. Contr.*, 37:485 – 490, 1990.

[27] E. L. Tan. Matrix Algorithms for Modeling Acoustic Waves in Piezoelectric Multilayers. *IEEE Trans. Ultrason. Ferroelect. Freq. Contr.*, 54 (10):2016–2023, 2008.

[28] E. L. Tan. Hybrid compliance-stiffness matrix method for stable analysis of elastic wave propagation in multilayered anisotropic media. *J. Acoust. Soc. Am.*, 119(1):45–53, 2006.

[29] T. M. Frederiksen and W. M. Howard. A single-chip monolithic sonar system. *IEEE Journal of Solid-State Circuits*, 9(6):394–403, December 1974.

[30] Billur Barshan. Fast processing techniques for accurate ultrasonic range measurements. *Measurement Science and Technology*, 11(1):45, 2000.

[31] Ali Safak Sekmen and Billur Barshan. Estimation of object location and radius of curvature using ultrasonic sonar. *Applied Acoustics*, 62(7):841 – 865, 2001.

[32] J. C. Jackson, R. Summan, G. I. Dobie, S. M. Whiteley, S. G. Pierce, and G. Hayward. Time-of-flight measurement techniques for airborne ultrasonic ranging. *IEEE Transactions on Ultrasonics, Ferroelectrics, and Frequency Control*, 60(2):343–355, February 2013.

[33] C. Knapp and G. Carter. The generalized correlation method for estimation of time delay. *IEEE Transactions on Acoustics, Speech, and Signal Processing*, 24(4):320–327, August 1976.

[34] J. Wang, D. Yuan, and P. Cai. Range resolution of ultrasonic distance measurement using single bit cross correlation for robots. In *Information and Automation (ICIA), 2010 IEEE International Conference on*, pages 917–923, June 2010.

[35] Y. Xu, Y. Li, Z. Qu, S. Jin, and C. Jiang. A TOF Estimation Method for Underwater Acoustic Signal in Confined Underwater Space. *J. Comput. Inf. Syst.*, 8(4):1689–1696, 2012.

[36] R. Queiros, F. Correa Alegria, P. Silva Girao, and A. Cruz Serra. Cross-Correlation and Sine-Fitting Techniques for High-Resolution Ultrasonic Ranging. *IEEE Transactions on Instrumentation and Measurement*, 59(12):3227–3236, December 2010.

[37] X. Li, S. Lin, J. Liang, Y. Zhang, H. Oigawa, and T. Ueda. Fiber-Optic Temperature Sensor Based on Difference of Thermal Expansion Coefficient Between Fused Silica and Metallic Materials. *IEEE Photonics Journal*, 4(1):155–162, February 2012.

[38] Chris J. Bell, Stuart Reid, James Faller, Giles D. Hammond, Jim Hough, Iain W. Martin, Sheila Rowan, and Kirill V. Tokmakov. Experimental results for nulling the effective thermal expansion coefficient of fused silica fibres under a static stress. *Classical and Quantum Gravity*, 31(6):065010, 2014.

[39] https://goochandhousego.com/product-categories/ln-wafers/.

[40] F. Pignatiello, M. De Rosa, P. Ferraro, S. Grilli, P. De Natale, A. Arie, and S. De Nicola. Measurement of the thermal expansion coefficients of ferroelectric crystals by a moiré interferometer. *Optics Communications*, 277(1):14 – 18, 2007.

[41] Nykolai Bilaniuk and George S. K. Wong. Speed of sound in pure water as a function of temperature. *The Journal of the Acoustical Society of America*, 93(3):1609–1612, 1993.